Subensemble decomposition and Markov process analysis of Burgers turbulence

Zhi-Xiong Zhang and Zhen-Su She

Phys. Rev. E **84**, 026326 — Published 25 August 2011

DOI: 10.1103/PhysRevE.84.026326

Sub-ensemble decomposition and Markov process analysis of Burgers turbulence

Zhi-Xiong Zhang* and Zhen-Su She
State Key Laboratory of Turbulence and Complex Systems
and College of Engineering, Peking University, Beijing 100871, P.R. China

A numerical and statistical study has been performed to describe the positive and negative local sub-grid energy fluxes in the one-dimensional random-force-driven Burgers turbulence (Burgulence). We use a sub-ensemble method to decompose the field into shock wave and rarefaction wave sub-ensembles by group velocity difference. We observe the shock wave sub-ensemble shows a strong intermittency which dominates the whole Burgulence field, while the rarefaction wave sub-ensemble satisfies K41 scaling law. We calculate the two sub-ensemble probabilities and find in the inertial range they keep scale-invariance, which is the important feature of turbulence self-similarity. We reveal the interconversion of shock and rarefaction waves during the equation's evolution displays in accordance with a Markov process, which having a stationary transition probability matrix with the elements satisfying universal functions and, when time interval is much greater than corresponding characteristic value, exhibiting the scale-invariant property.

PACS numbers: 47.27.Gs, 02.50.Ga, 47.27.eb

I. INTRODUCTION

One of the most important features of turbulence is the energy flux or the energy cascade, which has two transfer directions: from large to small scales – (positive) energy flux – derived by Kolmogorov for 3D turbulence [1], and from small to large scales – negative/inverse energy flux – proposed by Kraichnan for 2D turbulence [2]. These two physical processes exist in most of turbulence fields at same time from a local point of view suggested by Kraichnan [3]. Typically, in Burgers turbulence (abbreviated as "Burgulence" by Frisch and Bec [4]), a simplified approximation of Navier-Stokes equation, the positive and negative local energy fluxes are corresponding to shock wave and rarefaction wave, respectively. Now, the forced Burgulence has been at the center of studies that allowed unifying different branches of physics and mathematics [5]. Revealing the property of the local energy fluxes is one of the most fundamental problems in turbulence.

In 1939, the Dutch scientist J.M. Burgers introduced a 1D model for pressure-less gas dynamics [6], famously known as the Burgers equation

$$\frac{\partial u}{\partial t}+\frac{1}{2}\frac{\partial u^2}{\partial x}=\nu\frac{\partial^2 u}{\partial x^2}, \tag{1}$$

which is widely studied in statistical physics, cosmology, and hydrodynamical turbulence today. In the 1950s, Hopf [7] and Cole [8] demonstrated mathematically that Burgers equation can be integrated explicitly. Later, Meecham and Siegel [9], and Hosokawa and Yamamoto [10] numerically investigated this model with random initial values using Wiener-Hermite expansion and Hopf theory, respectively. While, its dynamical behavior is fundamentally different from the Navier-Stokes dynamics for the absence of pressure term and the local interactions only in x-space. To model the pressure, Jeng [11] imposed a random force $f(x,t)$ on the RHS of Eq. (1) and found the numerical velocity field satisfied quasi-Gaussian distribution and the energy spectrum $E(k)\propto k^{-2}$.

Soon after, many important efforts were devoted to the study of the solutions of Burgulence arising from random initial conditions or a random forcing. For the solution of inviscid Burgers equation with random initial data, Avellaneda and Weinan [12], who's work inspires us considering Markov process in this paper, rigorously proved some statistical properties for velocities, shock-strengths and rarefaction intervals. For the random forcing, based on Renormalization Group (RNG) methods, Forster, Nelson and Stephen [13] proposed a widely spread, white-in-time random, and zero mean formula in spectral space,

$$\langle\hat{f}(k,t)\hat{f}(k',t')\rangle=2(2\pi)^2Dk^{-1}\delta(k+k')\delta(t-t'), \tag{2}$$

where $\hat{\cdot}$ stands the Fourier representation.

In 1995, Chekhlov and Yakhot [14] numerically studied the random-force-driven Burgers equation again, where the viscous term was replaced by a hyperdissipation form $\nu(-1)^{p+1}\partial^{2p}u/\partial x^{2p}$ and a special group of random forcing parameters were employed. They obtained a remarkable result that the dynamics of the forced equation became more similar to that of Kolmogorov turbulence with a long inertial range, where energy flux was a constant as the viscosity goes to zero, energy spectrum satisfied Kolmogorov's $k^{-5/3}$ law [15], but the scaling law was different from the Kolmogorov's prediction $p/3$ [16] and indicated that the higher order correlation functions were still dominated by shocks. Recently, abundant numerical, statistical, and theoretical investigations on forced Burgulence, including the field theory results deduced by Polyakov [17], have been reported [17–27], in which many features such as asymmetry probability distribution, anomalous scaling law and strong intermittence etc., are discussed deeply.

* pekingzzx@pku.edu.cn

Here, we focus on the statistical scaling behavior and Markov process evolution of Burgulence's shock and rarefaction waves, which are corresponding to the positive and negative sub-grid scale energy fluxes, respectively. Sect.II is a sketch about the Burgulence fields generated using Chekhlov and Yakhot's method [14]. In Sect. III, a new sub-ensemble decomposition are used to distinguish the shock wave from rarefaction wave at different scales, and two different scaling laws are shown, which evinces that the shock wave ensemble has a strong intermittency which dominates the Burgulence intermittency, while the scaling behavior of the rarefaction wave ensemble satisfies K41 theory. In Sect. IV, after certifying the scale-invariance of sub-ensemble probabilities, we reveal the interconversion of shock and rarefaction waves during the equation's evolution displays in accordance with a Markov process, which having a stationary transition probability matrix with the elements satisfying universal functions and, when time interval is much greater than corresponding characteristic value, exhibiting the scale-invariant property. At last, the effects of random forcing parameter y are represented in Sect. V.

II. DNS FOR BURGULENCE

Using the Fourier-Galerkin pseudospectral method described in [14], the direct numerical simulation (DNS) for constructing Burgulence field is sketched as follows. As the governing equation of velocity signal $u(x,t)$, the random-force-driven Burgers equation writes

$$\frac{\partial u}{\partial t}+\frac{1}{2}\frac{\partial u^2}{\partial x}=\nu(-1)^{p+1}\frac{\partial^{2p}u}{\partial x^{2p}}+f, \tag{3}$$

where $p=6$ and $\nu=9.0\times10^{-40}$ which are set mainly for getting a long inertial range. To apply the Fourier-Galerkin pseudospectral method, periodic boundary conditions, $\partial^n u(0,t)/\partial x^n=\partial^n u(2\pi,t)/\partial x^n,\ n=0,1\cdots$, are imposed on the computational domain $x\in[0,2\pi]$.

Then, the random force satisfying Eq.(2) in Fourier space is given as

$$\hat{f}(k,t)=\begin{cases}\dfrac{A_f|k|^{-y/2}\sigma_k}{\sqrt{\Delta t}} & k<k_c,\\ 0 & k\geqslant k_c,\end{cases} \tag{4}$$

where σ_k is the Gaussian random function with $\overline{|\sigma_k|^2}=1$, and other parameters are chosen to be $A_f=\sqrt{2}\times10^{-3}$ and $y=1$. The force cutoff k_c is chosen well inside the dissipation range of the energy spectrum, with $k_c=3895$. The time step is set as $\Delta t=5.0\times10^{-5}$.

When implementing the algorithm, the initial field is given by a sine function, $u(x,0)=0.08\sin(x)$. The temporal discretization includes two second-order schemes: Runge-Kutta for restarting and stiffly stable Adams-type scheme with the explicit formulation as

$$\hat{u}(k,t+\Delta t)=\hat{u}(k,t)+\frac{3}{2}\Delta t\cdot\hat{g}(k,t)-\frac{1}{2}\Delta t\cdot\hat{g}(k,t-\Delta t), \tag{5}$$

where $\hat{g}(k,t)=\hat{f}(k,t)-ik\widehat{[u^2]}(k,t)/2-\nu k^{2p}\hat{u}(k,t)$.

During the computing, the spatial discretization is based on the pseudospectral method with the nonlinear $\widehat{[u^2]}$ computation in the conservative form and dealiasing procedure based on the 2/3 rule. The spectral resolution employed here is $N=12288$ including the de-aliased modes, and the random force generated at different computing time is non-repeating.

As results, the velocity field at $t=300$ and the average energy spectrum with $t\in[100,300]$ are shown in Fig.1 and Fig.2, respectively. In the plots, the typical fractal-like and sawtooth structures in velocity field and the Kolmogorov $k^{-5/3}$ spectrum with a long inertial range are reproduced, which conform well to the results in [14]. Here, we want to point out that the statistical features of shock and rarefaction waves depend on the random forcing much more than the initial data.

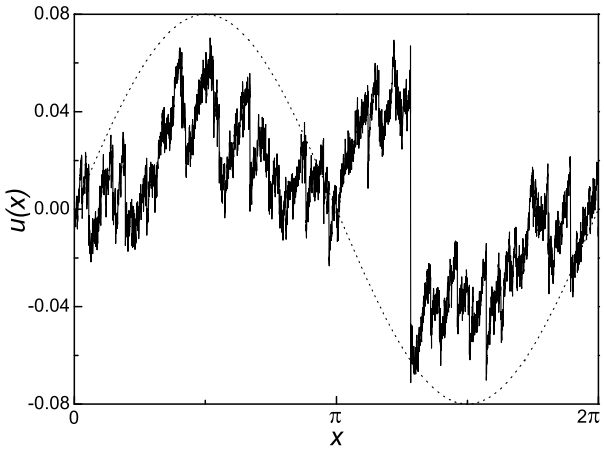

FIG. 1. Velocity signal of Burgers equation at $t=300$ (solid line) and $t=0$ (dot line, the initial field).

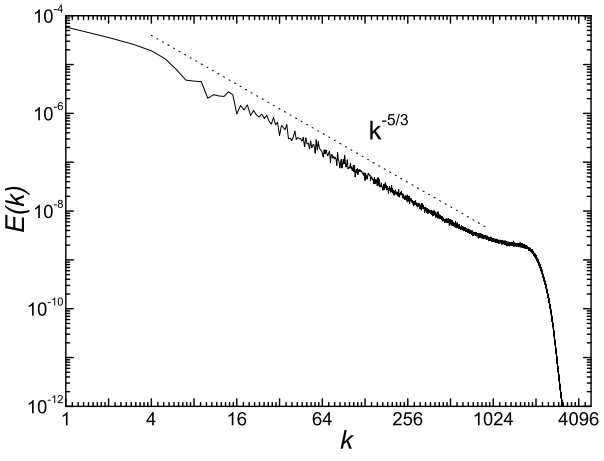

FIG. 2. Energy spectrum averaged in $t\in[100,300]$ (solid line). A dot line with slope $-5/3$ is also ploted.

III. SUB-ENSEMBLE DECOMPOSITION AND CORRESPONDING SCALING LAW

In traditional generalized opinion, the shock and rarefaction waves in 1D Burgulence, can be defined though the speed difference $\delta u(x,l) = u(x+l/2) - u(x-l/2)$, where $x+l/2$ and $x-l/2$ are the start and end locations of corresponding structure. If $\delta u(x,l) > 0$, the structure is regarded as rarefaction wave. On the contrary, if $\delta u(x,l) < 0$, the structure is belong to shock wave. From Burgers' results[28] on the distribution of the separations between rarefaction intervals and the Markovian nature of the equation solution, the set of shock locations, which have no thickness ($l \to 0$), is expected to be countable and discrete. In his case, the structure of shocks depends crucially on the similarity properties of the random initial data. While in the random-force-driven Burgulence, under the unceasing action of random forcing, the affection of initial data to the statistical features of shock and rarefaction waves becomes smaller and smaller. From Fig.1, we can see that the Burgulence field has typical fractal characteristic, since there is shocks in any arbitrary scale rarefaction wave.

Now, we introduce the concept of group velocity difference (GVD) denoted as $h(x,l)$ to identify "new" shock and rarefaction waves from a filtered field point of view. In mathematics, the GVD $h(x,l)$ can be written as difference of local integrations,

$$h(x,l) = \frac{2}{l}\int_0^{l/2} u(x+l')dl' - \frac{2}{l}\int_{-l/2}^{0} u(x+l')dl'. \quad (6)$$

Moreover, $h(x,l)$ has an equivalence definition as

$$h(x,l) = \frac{1}{l}\int_0^{l} \delta u(x,l')dl' = \delta\widetilde{u}(x,l/2), \quad (7)$$

where $\tilde{\cdot}$ stands a box filtering. Through the sign of $h(x,l)$, the fluctuation structures in the whole field can be divided into two sub-ensembles, namely,

$$J \in \begin{cases} A & h(x,l) \geqslant 0 \\ B & h(x,l) < 0. \end{cases} \quad (8)$$

Here, J marks the structure style; A and B denote the rarefaction wave and shock wave sub-ensembles, respectively. Fig.3 is a sketch of this definition: if its right half group/average velocity is larger or less than the left one, the structure in $[x-l/2, x+l/2]$ with l denoted as interval size or structure scale will be regarded as an element of sub-ensemble A or B.

No doubt, this decomposition is in accord with the common comprehension about the positive and negative local energy fluxes or energy cascade. Following Eyink's definition [29], we represent the local energy flux in Burgulence as $\Pi(x,l/2) = -(\widetilde{u^2} - \tilde{u}^2)\partial\tilde{u}(x,l/2)/\partial x$. Approximatively, there is $\Pi(x,l/2) \approx -2(\widetilde{u^2} - \tilde{u}^2)h(x,l)/l$, which means that when $h(x,l) < 0$, $\Pi(x,l/2) > 0$, the energy cascade is forward – from large to small scales; when $h(x,l) \geqslant 0$, $\Pi(x,l/2) \leqslant 0$, the energy cascade is reverse – from small to large scales.

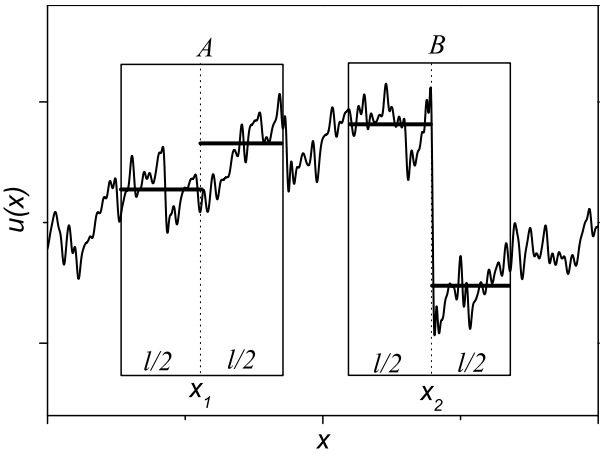

FIG. 3. A sketch for the definition of sub-ensemble A (rarefaction wave) and B (shock wave) using an enlarged segment in Fig.1 (solid line). The heavy horizontal lines in small boxes state the local group/average velocities.

Then, based on above sub-ensemble decomposition, we can investigate the scaling behaviors in each different sub-ensemble, respectively. Following the traditional method, we define the statistical moment function of $h(x,l)$ as

$$Z_p(l) = \langle |h(x,l)|^p \rangle, \quad (9)$$

where $\langle\cdot\rangle$ stands for ensemble average. From 20000 statistical stable velocity fields obtained in previous section with equal time interval and $t \in [100, 300]$ (without special explanation, all statistics in this paper are measured from the same 20000 velocity fields), $Z_p(l)$ for sub-ensemble A and B are measured and plotted in Fig.4 and Fig.5 with $l/\delta = 2, 4, \ldots, 1024$ and $p = 1, 2, \ldots, 8$ (δ is the physical resolution equaling to $2\pi/(2N/3)$ in DNS). The plots reveal that both sub-ensembles satisfy good absolute scaling law in an inertial range,

$$Z_p(l) \propto l^{\zeta_p}. \quad (10)$$

From Fig.4 and Fig.5, we can see both of sub-ensemble A and B have the same inertial range, the slope of line in log-log plot of Fig.4 is growing gradually with order number p increasing from 1 to 8, but the slopes of lines in Fig.5 change no more after a certain order number $p \approx 3$. Furthermore, we plot out these scaling exponents for sub-ensemble A, sub-ensemble B and whole field without decomposition in Fig.6. It's distinctly clear that the scaling behaviors in sub-ensemble A and B are very different from each other.

For sub-ensemble A, the scaling behavior is very approximative to K41 theorem [16] with

$$\zeta_{p,A}(l) = p/3, \quad (11)$$

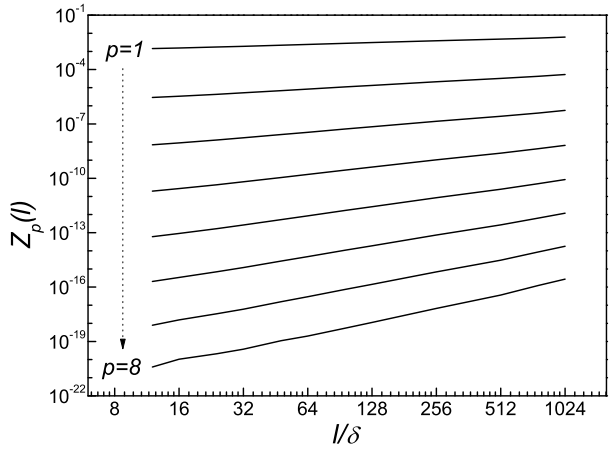

FIG. 4. Structure function for sub-ensemble A(solid line) at different scales $l/\delta = 12, 16, \ldots, 1024$.

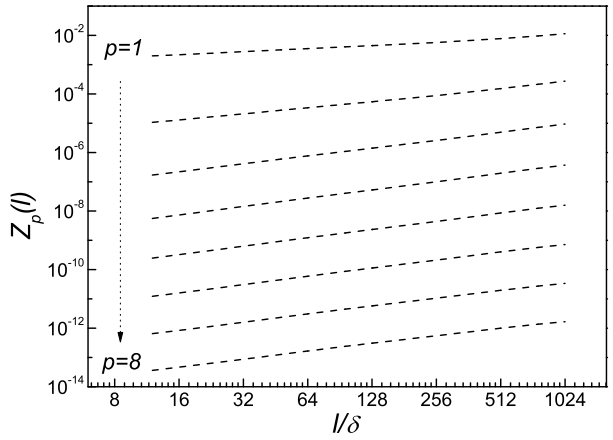

FIG. 5. Structure function for sub-ensemble B(dot line) at different scales $l/\delta = 12, 16, \ldots, 1024$.

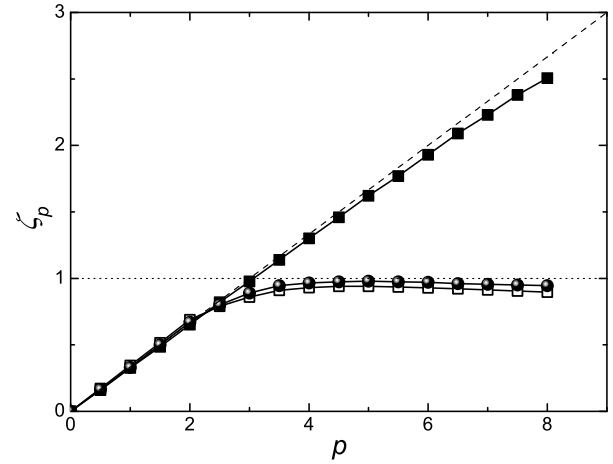

FIG. 6. Exponents of structure function for sub-ensemble A (fill squares), sub-ensemble B (open squares) and the whole field (fill circles). Dash line and dot line are corresponding to $\zeta_p = p/3$ and $\zeta_p = 1$, respectively.

which means sub-ensemble A has a conspicuous Gaussian property with little intermittence. For sub-ensemble B, an anomalous scaling law is observed:

$$\zeta_{p,B}(l) = p/3, p < 3; \quad \zeta_{p,B}(l) \approx 0.92, p > 3. \tag{12}$$

Evidently, it's more like the typical anomalous scaling law in Burgers equation and different from either K41 theory [16] or SL94 model [30]. The scaling exponents in the whole field with $\zeta_p(l) \sim 0.95$ when $p > 3$ are close to those in sub-ensemble B, since the the statistical moment function $Z_p(l)$ of sub-ensemble B is much larger than that of sub-ensemble A at same order number p, which can be confirmed through comparing Fig.4 with Fig.5. So it's surprisingly explicit that sub-ensemble B – shocks – dominate the intermittency of Burgulence.

As background, the typical anomalous scaling in Burgers equation has been obtained in [14], where the scaling exponents ζ_p of the ordinary velocity structure functions, defined by $S_p(l) = \langle |v(x+l) - v(x)|^p \rangle \propto l^{\zeta_p}$, were found to be almost independent of p, (ζ_p=0.91 at p=4,6,8). It is also noted that, Mitra et al.[27] argued that in the stochastically forced Burgers equation, they have found an artifact in which logarithmic corrections can appear disguised as anomalous scaling and conclude that bifractal scaling is likely. In fact, the probability distribution function (PDF) of $h(x,l)$ in A and B have different properties and the PDF of $h(x,l)$ in B also have algebraic tails, similar to the results discussed in [19, 22, 26].

Above results signal that, through sub-ensemble decomposition, the difference of shock and rarefaction waves within the same dynamical system – Burgulence– can be clearly revealed from corresponding statistical scaling behaviors. In other words, the two kinds of self-organization processes, the positive and negative local energy fluxes, in Burgulence have extremely different states: one has little intermittence, but another has strong intermittence; one has Gaussian property, but another does not. When they are mixed together, one of them may be obscured in the whole system behavior, which is witnessed by the scaling law shown Fig.6.

IV. MARKOV PROCESS EVOLUTION BETWEEN TWO SUB-ENSEMBLES

Based on the sub-ensemble definition above, we employ the Markov process analysis to describe the transition between the positive and negative local energy fluxes. For a velocity field u(x,t) at fixed t with $x \in [0, 2\pi]$, it's easy to count the probability of sub-ensemble at structure scale l,

$$P_A(l,t) = P(h(x,l,t) \geqslant 0 | x \in [0, 2\pi]); \tag{13}$$
$$P_B(l,t) = P(h(x,l,t) < 0 | x \in [0, 2\pi]). \tag{14}$$

Obviously, $P_A(l,t) + P_B(l,t) = 1$, and if sub-ensemble A and B have the same probability, there will be $P_A(l,t) = P_B(l,t) = 0.5$. But the truth of the matter is quite different.

In fact, $P_A(l,t)$ is distinctly greater than $P_B(l,t)$ at the statistical equilibrium state of Burgulenc, in which the probabilities have rarely changes after time $t = 100$, though they are fluctuating with time going forward. Fig.7 shows the time average probabilities of sub-ensemble A and B at different scales with error bars marked by the standard deviations. Here, the time average probabilities are $\langle P_A(l)\rangle = \int_{t_0}^{t_e} P_A dt/(t_e - t_0)$ and $\langle P_B(l)\rangle = \int_{t_0}^{t_e} P_B dt/(t_e - t_0)$, where $t_0 = 100, t_e = 300$. The plot illustrates that the probabilities are independent with l at a large scale range $10 < l/\delta < 600$:

$$\langle P_A(l)\rangle = 0.575; \quad \langle P_B(l)\rangle = 0.425.$$

Namely, the probabilities satisfy scale invariance in the inertial range, which is the important feature of self-similarity and is the basic of Markov process analysis below.

Markov process, named after the Russian mathematician Andrey Markov[31], is a time-varying random phenomenon for which a specific property (the Markov property) holds. The most famous Markov process is Markov chain. In real world, many processes are belong to the Markov process, such as the Brownian motion of particle in liquid, the animal number change in forest, the number of people infected by disease, the number of people waiting bus in station, the transition of free electron in atomic nucleus, the population growth, some courses of inheritance, and so on. After Markov, many famous theorist in probability, statistics, mathematics and physics etc have made important improvements on relative studies, such as Kolmogorov [32], Ito [33], Feller [34], Dynkin [35], Dvoretzky [36], and Hunt [37] etc.

Markov chain [38] is a sequence of stochastic variable, $X_1, X_2, X_3...$, with their range as state space gathering all of the possible value, where X_n denotes the state at time t_n. A stochastic process has the Markov property if the conditional probability distribution of future state X_{n+1} depends only upon the present state X_n; that is, given the present, the future does not depend on the past. This feature can be written with a probability form:

$$P(X_{n+1} = x|X_0, X_1, X_2, \ldots, X_n) = P(X_{n+1} = x|X_n).$$

During the Burgers equation evolution under the action of random forcing, the energy cascade at point x with fixed scale l will change between positive and negative direction. The transition appears as the interconversion of shock and rarefaction waves is a kind of Markov process. Fig.8 shows a sketch about this feature in the Eulerian sense. There are totally four kinds of structure style transitions between A and B: $A \rightarrowtail A$; $A \rightarrowtail B$; $B \rightarrowtail A$; and $B \rightarrowtail B$. The key quantities to describe Markov process are so-called transition probabilities defined as:

$$\begin{aligned} P_{AA}(l,t_1,\delta t) &= P(h(x,l,t_2) \geqslant 0|h(x,l,t_1) \geqslant 0), \\ P_{AB}(l,t_1,\delta t) &= P(h(x,l,t_2) < 0|h(x,l,t_1) \geqslant 0), \\ P_{BA}(l,t_1,\delta t) &= P(h(x,l,t_2) \geqslant 0|h(x,l,t_1) < 0), \\ P_{BB}(l,t_1,\delta t) &= P(h(x,l,t_2) < 0|h(x,l,t_1) < 0), \end{aligned} \tag{15}$$

where the time interval $\delta t = t_2 - t_1$.

For $P_{AB} \equiv 1 - P_{AA}$ and $P_{BA} \equiv 1 - P_{BB}$, we need to only focus on two variables defined in Eq.(15) such as P_{AA} and P_{BB}. Through statistical counting, we found that the transition probabilities are independent with the reference time point t_1 but depend only on the time interval δt at the stable state ($t_1 > 100$). The time average of P_{AA} and P_{BB} at different scale l and time interval δt are defined as:

$$\langle P_{AA}(l,\delta t)\rangle = \frac{1}{t_e - t_0}\int_{t_0}^{t_e} P_{AA}(l,t',\delta t)dt', \tag{16}$$

$$\langle P_{BB}(l,\delta t)\rangle = \frac{1}{t_e - t_0}\int_{t_0}^{t_e} P_{BB}(l,t',\delta t)dt', \tag{17}$$

where $t_0 = 100$ and $t_e = 300$. Fig. 9 shows that when $\delta t = 163$ in the inertial range, like the probability of A and B, the four time average transition probabilities are scale-invariance, too. In fact, for a small time interval δt, the transition probability scale-invariance is untenable.

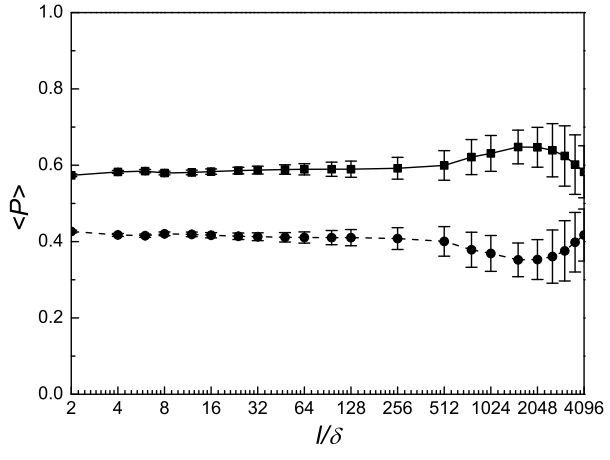

FIG. 7. Time average probabilities for sub-ensemble A (squares) and sub-ensemble B (dots) at different scales. The corresponding error bars are also plotted.

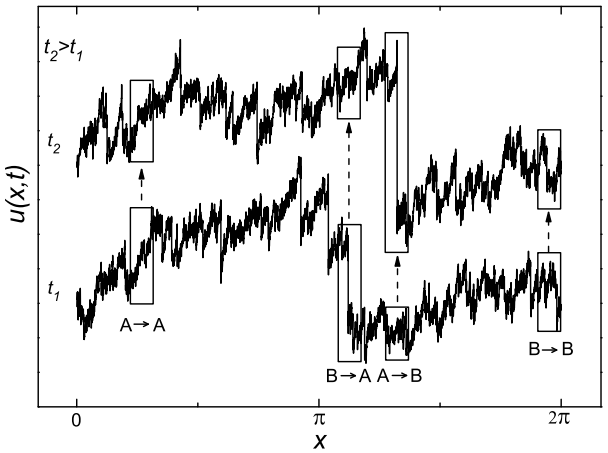

FIG. 8. Transitions between sub-ensemble A and B from t_1 to t_2 with fixed structure scale in the Eulerian sense.

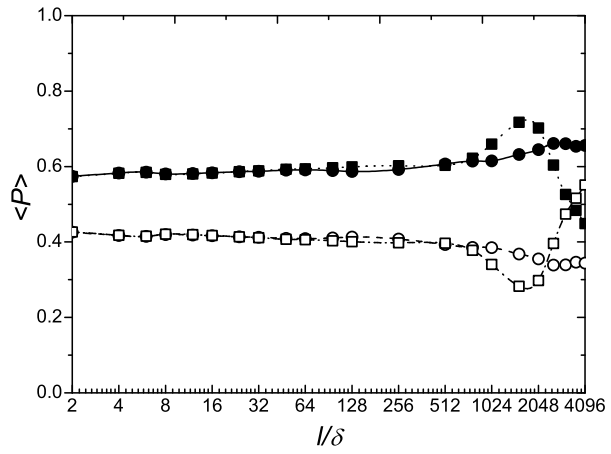

FIG. 9. Time average of transition probabilities: $\langle P_{AA}(l,\delta t)\rangle$ (fill squares); $\langle P_{AB}(l,\delta t)\rangle$ (fill circles); $\langle P_{BB}(l,\delta t)\rangle$ (open squares); and $\langle P_{BA}(l,\delta t)\rangle$ (open circles).

Fig. 10 and Fig. 11 display the changing of $\langle P_{AA}(l,\delta t)\rangle$ and $\langle P_{BB}(l,\delta t)\rangle$, respectively, with different time interval δt at different scales. Though the transition probability scale-invariance is broken at a fixed small δt, we can see, all of the transition probabilities possess a same similarity, which expresses the probabilities gradually converge towards 1 when $\delta t \to 0$ and towards a constant when $\delta t \to +\infty$. As a simple explanation, the value $\langle P_{AA}(l,\delta t\to 0)\rangle \approx 1$ or $\langle P_{BB}(l,\delta t\to 0)\rangle \approx 1$ indicates the time is too short to change the structure style from one to another.

To inspect the transition probability similarity, let us introduce the Chapman-Kolmogorov equation, which is often used to describe Markov chain,

$$\begin{pmatrix} P_A(l,t_2) \\ P_B(l,t_2) \end{pmatrix} = \begin{pmatrix} P_{AA}(l,t_1,\delta t) & P_{BA}(l,t_1,\delta t) \\ P_{AB}(l,t_1,\delta t) & P_{BB}(l,t_1,\delta t) \end{pmatrix} \begin{pmatrix} P_A(l,t_1) \\ P_B(l,t_1) \end{pmatrix}. \quad (18)$$

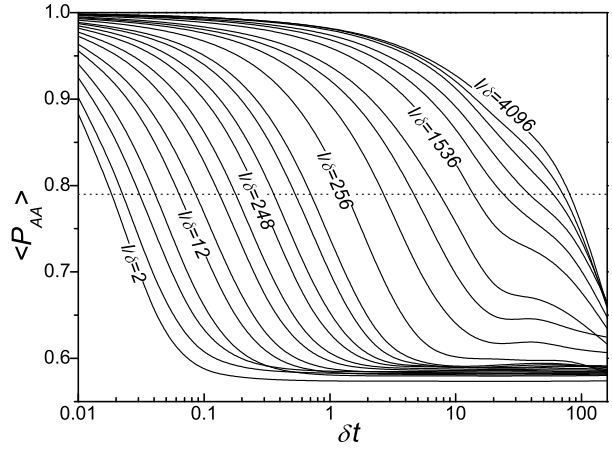

FIG. 10. Time average of transition probabilities $\langle P_{AA}(l,\delta t)\rangle$. The dot line is corresponding to $\langle P_{AA}\rangle = (1+\langle P_A\rangle)/2$.

Considering in the inertial range $10 < l/\delta < 600$,

$$P_A(l,t_1) \approx P_A(l,t_2),$$
$$P_B(l,t_1) \approx P_B(l,t_2),$$
$$P_{AB}(l,t_1,\delta t) = 1 - P_{AA}(l,t_1,\delta t),$$
$$P_{BA}(l,t_1,\delta t) = 1 - P_{BB}(l,t_1,\delta t),$$

and using the time average form, we can derive a new simple equation replacing Eg. (18),

$$\begin{pmatrix} \langle P_A(l)\rangle \\ \langle P_B(l)\rangle \end{pmatrix} = \begin{pmatrix} \langle P_{AA}(l,\delta t)\rangle & 1-\langle P_{BB}(l,\delta t)\rangle \\ 1-\langle P_{AA}(l,\delta t)\rangle & \langle P_{BB}(l,\delta t)\rangle \end{pmatrix} \begin{pmatrix} \langle P_A(l)\rangle \\ \langle P_B(l)\rangle \end{pmatrix} \quad (19)$$

Fig. 10 and Fig. 11 also tell us that when $\delta t \to +\infty$, $\langle P_{AA}(l,+\infty)\rangle \approx \langle P_A(l)\rangle$ and $\langle P_{BB}(l,+\infty)\rangle \approx \langle P_B(l)\rangle$, which is just right a group solution of Eq.(19). Similarly, $\langle P_{AA}(l,0)\rangle \approx 1$ and $\langle P_{BB}(l,0)\rangle \approx 1$ are another group solution of Eq.(19). Meanwhile, the speeds of the transition matrixes going to above two special solutions are different at different structure scales.

Here, we define a so-called characteristic time $\delta t^*(l)$ to normalize $\langle P_{AA}(l,\delta t)\rangle$ and $\langle P_{BB}(l,\delta t)\rangle$, respectively. For example, the characteristic time $\delta t^*(l)$ is equal to the horizontal ordinate value of crossing points between the line $\langle P_{AA}\rangle = (1+\langle P_A\rangle)/2$ and the lines $\langle P_{AA}(l,\delta t)\rangle$ in Fig. 10. The measured characteristic times at different l/δ are shown in Fig. 12 and markedly satisfy line functions with slop close to 1 in the inertial range,

$$\delta t^*(l) = C_t (l/\delta)^{\alpha}, \quad 10 < l/\delta < 600, \quad (20)$$

where $\alpha \approx 1$ and C_t is a system parameter.

Using the data in Fig. 12, we redraw Fig. 10 and Fig. 11 again into Fig. 13, where the horizontal ordinate are replaced by $\delta t/\delta t^*$. Clearly, all the transition probabilities, $\langle P_{AA}\rangle$ and $\langle P_{BB}\rangle$, collapse together as two curves with specific lower bounds, which satisfy the function

$$\langle P_{\beta\beta}(l,\delta t)\rangle = (1-\langle P_\beta(l)\rangle)\left(\frac{1}{2}\right)^{\delta t/\delta t^*(l)} + \langle P_\beta(l)\rangle, \quad (21)$$

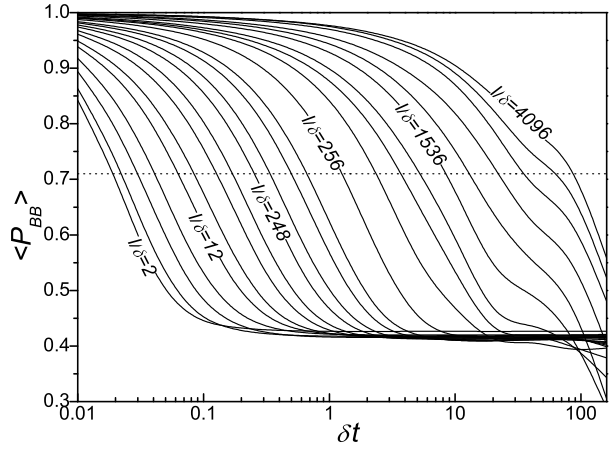

FIG. 11. Time average of transition probabilities $\langle P_{BB}(l,\delta t)\rangle$. The dot line is corresponding to $\langle P_{BB}\rangle = (1+\langle P_B\rangle)/2$.

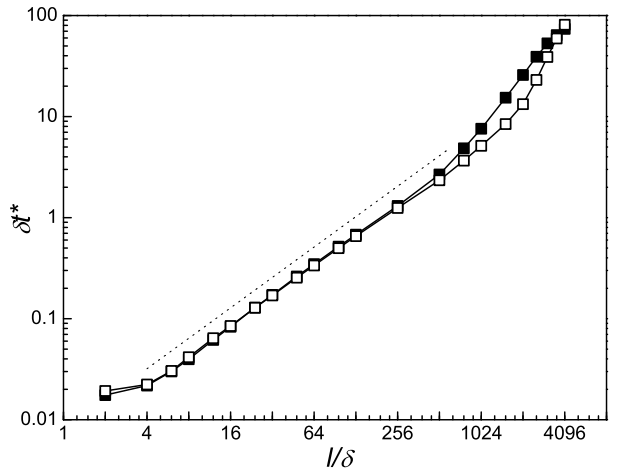

FIG. 12. Characteristic time of transition probabilities $\langle P_{AA}\rangle$ (fill squares) and $\langle P_{BB}\rangle$ (open squares) at different structure scale l. The dot line has a slope 1.

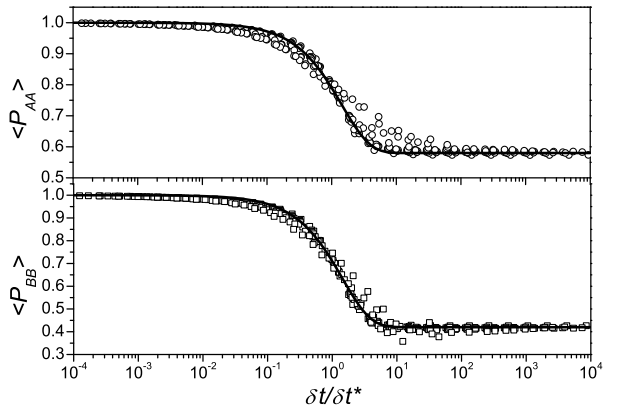

FIG. 13. Transition probabilities $\langle P_{AA}(l,\delta t/\delta t^*)\rangle$ (top) and $\langle P_{BB}(l,\delta t/\delta t^*)\rangle$ (down). The sold lines are corresponding to Eq. (21).

where β represents A or B. In the plot, some points departing from the curves are those out of the inertial range.

So based on the stationary transition probability matrix, $\langle P_{\beta\beta}(l,\delta t)\rangle \approx P_{\beta\beta}(l,\delta t)$, a collapsed Markov chain [39] have been built in fact. The probability $\langle P_\beta\rangle$ in Eq.(21) is found to depend mainly on the random force $f(x,t)$, especially the spectral exponent y in Eq.(5).

V. EFFECTS OF RANDOM FORCING PARAMETER y

In order to probe the effects of random forcing on the Burgulence field, we carried out five DNS cases with parameter $y = 0.25, 0.5, 0.75, 1.0, 2.0$ in Eq.(5), respectively and the others computation conditions are set identically as the case $y = 1.0$ discussed above. Using the sub-ensemble decomposition method explained in Sect. III, we obtained some statistical results for each case shown in Tab. I .

TABLE I. DNS cases and statistical quantities for Burgulence with different parameter y.

Case	y	$E(k)$	Slope of $\zeta_{p,A}$	$\langle P_A\rangle$
1	0.25	$\propto k^{-1.209}$	0.137	0.523
2	0.50	$\propto k^{-1.402}$	0.200	0.537
3	0.75	$\propto k^{-1.545}$	0.273	0.556
4	1.00	$\propto k^{-1.657}$	0.334	0.575
5	2.00	$\propto k^{-2.005}$	0.630	0.664

Fig. 14 shows the energy spectra of the five Burgulence fields. In the plot, the slopes of log-log plot energy spectra in inertial range is a monotone decreasing function of y, which deviates from Yakhot's prediction, $E(k) \propto k^{-5/3+2/3(d-y)}$, deduced in [40], where the dimension $d = 1$. When y is large, e.g. $y = 2.0$, the velocity field is close to a decaying Burgulence field with energy spectrum slope -2, which means the random forcing effect can be ignored. On the other hand, when y becomes smaller, the random forcing is bigger, the velocity field seems more like white noise, and the energy spectrum is flatter. Furthermore, a demonstrable proposition is that: when the energy spectrum becomes flatter and flatter, the entire average local energy flux at same scale becomes less and less referring to the total kinetic energy, which indicates the relative difference between the average positive and negative local energy fluxes is smaller. So when y is small enough, the phenomenon of the whole field being dominated by shock is no longer apparent.

Another important and interesting result is that, all of the exponents for sub-ensemble A exhibit linear scaling behaviors, and the slopes of $\zeta_{p,A}$ vs p form a monotone increasing function of y within inertial range,

$$\zeta_{p,A} \approx \frac{yp}{3},$$

which is shown in the insert of Fig. 15. At the same

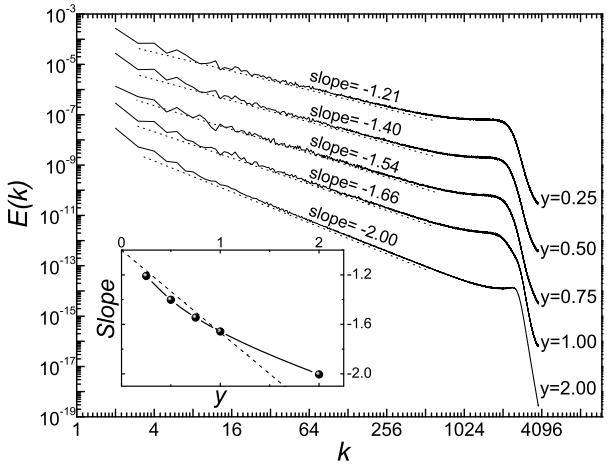

FIG. 14. Energy spectrum averaged in $t \in [100, 300]$ (solid line) with $y = 0.25, 0.5, 0.75, 1.0, 2.0$ respectively. The slopes are plotted in the inset, in which the dot line show Yakhot's prediction.

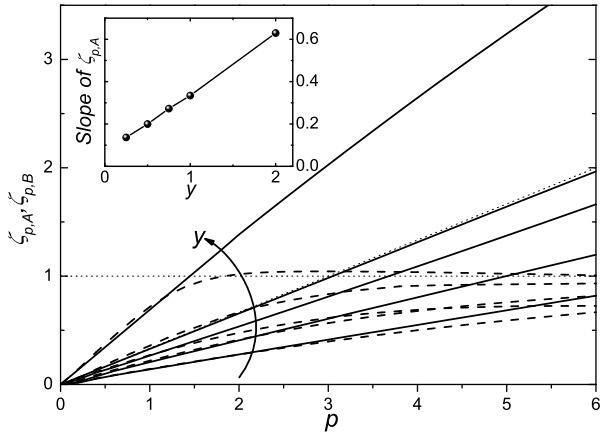

FIG. 15. Exponents of structure function for sub-ensemble A (solid lines) and sub-ensemble B (dash lines) with y increasing in the direction of the arrow. The horizontal dot line and the incline oblique dot line are corresponding to constant 1 and $p/3$ respectively. The inset shows the slopes of $\zeta_{p,A}$ vs y.

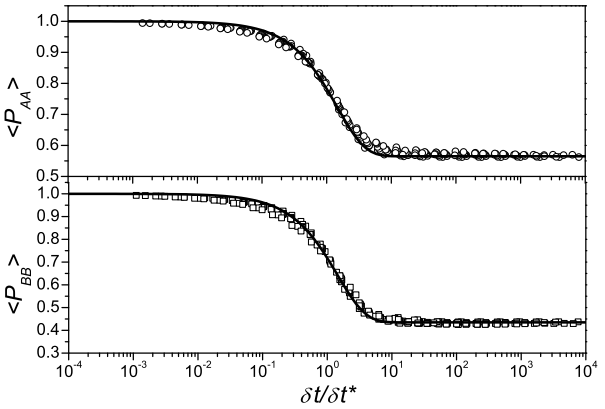

FIG. 16. Transition probabilities $\langle P_{AA}(l, \delta t/\delta t^*)\rangle$ (top) and $\langle P_{BB}(l, \delta t/\delta t^*)\rangle$ (down) with $y = 0.75$. The sold lines are corresponding to Eq. (21).

time, we can see from Fig. 15, the scaling behaviors of sub-ensemble B in all of the five cases are anomalous. The exponents of sub-ensemble B converge towards a different constant with different y at high orders p. Thus the shock waves, the positive energy fluxes, dominate the intermittency of Burgulence, but the domination level is lower when y is small, at the case of which the scaling behaviors of sub-ensemble A and B are close together. By the way, the total kinetic energy is at a high level with the same other conditions, though the relative energy fluxes is small at small y, when the field receives its statistical equilibrium.

At last, following the Markov analysis in Sect. IV, we obtained the collapsed time average transition probabilities $\langle P_{AA}(l, \delta t/\delta t^*)\rangle$ and $\langle P_{BB}(l, \delta t/\delta t^*)\rangle$ shown in Fig. 16 for the case $y = 0.75$. In this case, the relationship of Eq. (21) is still holden with new different parameters, which is mainly corresponding to the characteristic times and the sub-ensemble probabilities. Considering on the comparison among the five cases, we can conclude that: the smaller y is, the more the random forcing dominate the Burgulence field, the smaller the probability of sub-ensemble A is, and the smaller the characteristic time changing from one state to another is.

VI. CONCLUSION AND DISCUSSION

This paper presents a new description of the transition between the positive and negative local energy fluxes, or the shock and rarefaction waves, from the angle of sub-ensemble decomposition. Using the concept of group velocity difference (GVD), we divide Burgulence field into sub-ensemble A and B corresponding to rarefaction wave and shock wave. These two sub-ensembles possess probability scale-invariance in the inertial range and show K41 scaling law and typical Burgers anomalous scaling law respectively, which are corresponding to two different energy flux or cascade processes. Furthermore, we investigate the interconversion between A and B through Markov process analysis, and find the elements of the transition probability matrix in the stationary Chapman-Kolmogorov equation Eq. (19) fit a universal form at different scales, namely Eq. (21), which offers an uncomplicated probabilistic description for the structure evolution and exhibits some new properties of nonlinear dynamic self-organization in Burgulence.

Since the similarities between in 1D Burgulence and 3D Navior-Stocks turbulence, the statistical analysis method proposed here can be applied upon 3D turbulence, too. In 3D case, the local energy flux can be defined as [29]:

$$\Pi(\mathbf{x}, l) = -\frac{\partial \langle u_i\rangle_l}{\partial x_j}\tau_{ij} = -\frac{\partial \langle u_i\rangle_l}{\partial x_j}(\langle u_i u_j\rangle_l - \langle u_i\rangle_l\langle u_j\rangle_l),$$

where $\langle\cdot\rangle_l$ denotes the average at scale l. For the integral energy flux is nonzero, the distribution of local energy fluxes will be asymmetric about zero, and the scaling behaviors may be different in the two sub-ensembles corresponding to positive and negative sign of $\Pi(\mathbf{x}, l)$, respectively.

Another important issue is introducing the Lagrangian description to study the Markov process of sub-ensemble transition process, which will display a similar and more physical visualized pattern, we think. In addition, the two kinds of different cascade properties indicate that a new large eddy simulation (LES) may be erected based on the sub-ensemble decomposition idea. Beyond statistical theory, the concept itself of ensemble or sub-ensemble decomposition in the sense of self-organization [41] offers a simple hydrodynamical training ground for developing mathematical tools to study not only turbulence but also multi-structure, multi-scale, multi-state or Lagrangian problems.

ACKNOWLEDGEMENT

This work is supported by National Science Foundation of China (No. 90716008) and the MOST of China (973 project No. 2009CB724100). The authors wish to thank Y. Shi, M. Zhou, J. Chen, H. Guo, K. Ding, Y. Wang etc. for helpful discussions.

[1] A. N. Kolmogorov, Dokl. Akad. Nauk SSSR **32**, 16 (1941).
[2] R.H. Kraichnan, Phys. Fluids **10**, 2080 (1967).
[3] R.H. Kraichnan, J. Fluid Mech. **62**, 305 (1974).
[4] U. Frisch and J. Bec, "Burgulence", Les Houches 2000, edited by M. Lesieur, Springer EDP-Sciences, 341 (2001).
[5] J. Bec and K. Khanin, Phys. Rep. **447**, 1 (2007).
[6] J. M. Burgers, Kon. Ned. Akad. Wet. Verh. **17**, 1 (1939).
[7] E. Hopf, Commun. Pure Appl. Math. **3**, 201 (1950).
[8] J.D. Cole, Q. Appl. Math. **9**, 225 (1951).
[9] W. C. Meecham and A. Siegel, Phys. Fluids **7**, 1178 (1964).
[10] I. Hosokawa and K. Yamamoto, Phys. Fluids **13**, 1683 (1970).
[11] D. T. Jeng, Phys. Fluids **12**, 2006 (1969).
[12] M. Avellaneda and W. E, Commun. Math. Phys. **172**, 13 (1995); M. Avellaneda, Commun. Math. Phys. **169**, 45 (1995).
[13] D. Forster, D. R. Nelson, and M. J. Stephen, Phys. Rev. Lett. **36**, 876 (1976); D. Forster, D. R. Nelson, and M. J. Stephen, Phys. Rev. A **16**, 732 (1977).
[14] A. Chekhlov and V. Yakhot, Phys. Rev. E **51**, R2739 (1995); A. Chekhlov and V. Yakhot, Phys. Rev. E **52**, 5681 (1995).
[15] A. N. Kolmogorov, Dokl. Akad. Nauk SSSR **30**, 9 (1941).
[16] A. N. Kolmogorov, Dokl. Akad. Nauk SSSR **31**, 538 (1941).
[17] A. M. Polyakov, Phys. Rev. E **52**, 6183 (1995).
[18] J. P. Bouchaud, M. Mézard, and G. Parisi, Phys. Rev. E **52**, 3656 (1995).
[19] V. Yakhot and A. Chekhlov, Phys. Rev. Lett. **77**, 3118 (1996).
[20] O. Zikanov, A. Thess, and R. Grauer, Phys. Fluids **9**, 1362 (1997).
[21] V. Yakhot, Phys. Rev. E. **57**, 1737 (1998).
[22] Weinan E and E. Vanden Eijnden, Phys. Rev. Lett. **83**, 2572 (1999).
[23] A. I. Chernykh and M. G. Stepanov, Phys. Rev. E **64**, 026306 (2001).
[24] J. Bec, U. Frish, and K. Khanin, J. Fluid Mech. **416**, 239 (2000).
[25] J. Bec, Phys. Rev. Lett. **87**, 104501 (2001).
[26] S. Boldyrev, T. Linde, and A. Polyakov, Phys. Rev. Lett. **93**, 184503 (2004).
[27] D. Mitra, J. Bec, R. Pandit, and U. Frisch, Phys. Rev. Lett. **94**, 194501 (2005).
[28] J. M. Burgers, *The Nonlinear Diffusion Equation* (Reidel, Boston, 1974).
[29] G. L. Eyink, J. Stat. Phys., **78**, 335 (1995).
[30] Z. S. She and E. Leveque, Phys. Rev. Lett. **72**, 336 (1994).
[31] A. A. Markov, Izv. Fiz.-Matem. Obsch. Kazan Univ. **2**, 135 (1906).
[32] A. N. Kolmogorov, Math. Ann. **104**, 415 (1931); A. N. Kolmogorov, Math. Ann. **112**, 155 (1936).
[33] K. Ito, Mem. Am. Math. Soc. **4**, 51 (1951).
[34] W. Feller, Trans. Am. Math. Soc. **77**, 1 (1954); W. Feller, Ann. Math. **60**, 417 (1954).
[35] E. B. Dynkin, Theor. Probab. Appl. **1**, 22 (1956); E. B. Dynkin, Theor. Probab. Appl. **1**, 34 (1956).
[36] A. Dvoretzky, P. Erdös, and S. Kakutani, Acta Sci. Math. **12**, 75 (1950); A. Dvoretzky, P. Erdos, and S. Kakutani, Proc. Fourth Berkeley Symposium **2**, 103 (1961).
[37] G. A. Hunt, Illinois J. Math. **1**, 44 (1957).
[38] A. A. Markov, "Extension of the limit theorems of probability theory to a sum of variables connected in a chain." reprinted in Appendix B of: R. Howard. Dynamic Probabilistic Systems, volume 1: Markov Chains. John Wiley and Sons, (1971).
[39] J. Hachigian, Ann. Math. Stat. **34**, 233 (1963).
[40] V. Yakhot and S. A. Orszag, J. Sci. Comput. **1**, 3 (1986).
[41] Z. S. She and Z. X. Zhang, Acta Mech. Sin. **25**, 279 (2009).